Thermal Science and Engineering Progress 47 (2024) 102322

Contents lists available at ScienceDirect

Thermal Science and Engineering Progress

journal homepage: www.sciencedirect.com/journal/thermal-science-and-engineering-progress

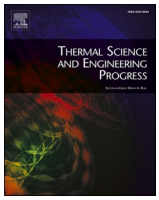

Performance prediction of single-pass and multi-pass low-cost solar air heater

Emmanuel Omotosho [a,*], Philip Hackney [b]

[a] Durham Business School, Durham University, Durham, UK
[b] Faculty of Engineering and Environment, University of Northumbria, Newcastle Upon Tyne, UK

ARTICLE INFO

Keywords:
Low-cost solar heater
Solar absorber
Solar air heater
Multi-pass

ABSTRACT

This study introduces a mathematical model and experimental evaluation of solar air heating utilising an absorber surface constructed from low-cost upcycled materials. The research presents a solar air heater prototype, suitable for applications such as space heating and agricultural drying. The solar heating system was modelled using upcycled beverage aluminium cans, considering both single and multi-pass flow configurations. Performance in terms of useful heat was determined through both mathematical model simulations and experimental methods. The multi-pass system demonstrated superior performance, delivering increased usable heat at elevated temperatures compared to the single-pass system. A comparative analysis and validation were conducted between numerical investigations with natural and forced convection on the five-pass solar air heater and experimental test outcomes. This research highlights the potential of utilising waste materials to develop cost-effective, solar heating solutions, contributing to energy management and waste reduction strategies. The findings can be explored for future explorations into sustainable and renewable energy solutions, particularly beneficial in regions with constrained economic resources.

1. Introduction

The use of fossil fuels and their effect on climate are well-recognised [32,1]. Coupled with the increased pressure from population, economic and industrial growth, researchers are seeking more effective means of harvesting solar energy [18]. Solar energy remains one of the most attractive energy sources as it is clean, free, predictable, and abundantly available [24]. A solar air heating system is one of the few highly efficient methods for converting solar energy to thermal energy, as reported by Bhatt and Yadav [9,42]. The design of solar air heaters significantly influences their performance. According to literatures [3;8], solar air heaters can be classified into passive, hybrid, or active types. The main characteristic that differentiates solar air heaters is the air ducts, which may either inhibit or enhance heat transfer and turbulence rate [38]. Solar air heating with non-restrictive material is considered to have low thermal efficiency due to ineffective heat transfer between the absorber plate and the air duct [12,3]. Hassan et al. [22] presented the tubular solar air heater, where adjacent tubes were used to achieve an efficiency of 83.6 % at an air mass flow rate of 0.075 kg/s. This performance represented a 10–15 % efficiency increase compared to the existing solar air heater at the time of the study. Potgieter et al. [33] presented a solar air heater with an energy conversion rate between 23 % and 83 % at an air mass flow rate of 0.00321 kg/s. Another approach involves using phase change material for heat storage, which mainly enhances night usage [29,36,25]. Other techniques employ artificial roughness [19;20;34], porous/packed bed [39,35] to increase the heat delivery of the solar air heaters. However, the major drawbacks of the current solar air heaters are their intricate design and the cost of setup.

In this study, we focus on investigating the cost and performance of developing a simple solar air heater using waste aluminium cans. While there are existing publications on solar air heaters using beverage cans [28,30,14], this study contributes to the field by providing a comprehensive mathematical and performance analysis that is validated with experimental tests. This research not only fills a gap in the current literature but also offers a model that can be utilised for future investigations. In this setup, the solar air heater is developed using upcycled Pepsi cans and medium-density fibreboard (or wood) to hold the cans together. The aluminium beverage cans serve as both the absorber plate and the air duct, with the lids and bases removed and arranged as the duct for the air pathway. Murali et al. [30] studied the air inlet and outlet temperature difference and heat transfer coefficient using aluminium cans with aluminium scraps and pebble stones. The study revealed that the outlet temperature was 1.5 K higher than the

* Corresponding author.
E-mail addresses: emmanuel.o.omotosho@durham.ac.uk (E. Omotosho), phil.hackney@northumbria.ac.uk (P. Hackney).

https://doi.org/10.1016/j.tsep.2023.102322
Received 19 June 2023; Received in revised form 26 October 2023; Accepted 3 December 2023
Available online 13 December 2023

Nomenclature

A	the contact area for each fluid side (m^2) (with A1 and A2 expressing either surface)
f	fanning friction factor
h	individual heat transfer coefficient (W/m^2K)
h_w	heat transfer coefficient due to wind flowing over the glass cover (W/m^2K)
$\dot{h}$	convective heat transfer coefficient (W/m^2K)
$\overline{h}$	radiative heat transfer coefficient (W/m^2K)
I	Solar radiation intensity (W/m^2)
Lb	distance between glass cover and absorber plate (m)
$\dot{m}$	mass flow rate of air (kg/s)
Nu	Nusselt number
q	Heat transfer per unit area (W/m^2)
Pr	Prandtl's number
Ra	Rayleigh number
Re	Reynolds number
T	temperature (K)
Va	is the mean air velocity (m/s)
Vw	Velocity of wind (m/s)
U	heat loss coefficients (W/m^2K)
Δx	the wall thickness (m)

Greek letters

γ	Absorptivity
ε	Emissivity
μ	is the dynamic viscosity
λ	Thermal conductivity (W/(m·K))
v_{air}	Kinematic viscosity (m^2/s)
ρ	is the density of air
τ	transmissivity
φ_{air}	Thermal diffusivity (m^2/s)
x_c	Thickness of the aluminium can (m)

Sub-scripts

a	Energy flow between topside (c) to bottom-side (e) of aluminium Can
am	ambient air
b	Energy flow between glass cover (g) and Aluminium Can topside (c)
c	aluminium can (top side)
d	Energy flow between glass cover (g) and ambient air (am)
e	aluminium can (bottom side)
g	glass cover
i	insulation (medium-density fibreboard)
w	wind flow

ambient temperature after sunset when used with a solar storage material. Mgbemene et al. [28] presented experimental results of using aluminium cans. With an average irradiance of 800 W/m^2 and an ambient temperature of 30 °C, outlet temperatures of 80 °C and 128 °C for a single-pass and four-pass air heater respectively were achieved, but no validation was presented for the study. This study seeks to address this by investigating the performance of both single and multi-pass solar air heaters using mathematical simulation, and validating these simulations with experimental results.

The purpose of this study is to;

a) Develop a mathematical model of a beverage aluminium solar air heater.
b) Compare the mathematical model with experimental results.
c) Investigate the performance of single-pass and multi-pass solar air heater configurations.

2. Materials and methods

2.1. Design configuration

Mgbemene et al. [28] used aluminium drink cans as a solar absorber to illustrate, using experimental results, that an outlet temperature of 80 °C and 128 °C was possible for a single-pass and four-pass air heater, respectively. The mass flow rate for the four-pass air heater was less than that of the single-pass air heater, although the air temperature of the four-pass air heater was higher. The solar irradiance at the point of reading and the generated heat energy were not stated The solar absorber cans had their outside surface painted with matte black chalkboard paint to improve solar gain for the exposed surfaces only. The aperture of the cans was increased to allow free air flow between each can stack in the array. The absorber tubes were contained in a wood frame configured to channel and guide the flow of air through the array and a Perspex cover to reduce energy loss by convection, as shown in Fig. 1 and Fig. 2. The design specification and measurements for the setup are presented in Fig. 3.

Table 1 consists of the material used for the setup, and the total cost was estimated to be $63.86 using pricing from eBay at the time the experiment was conducted. The blower fan employed for the experiment is a used laptop CPU fan and can be found on eBay for as low as $2.

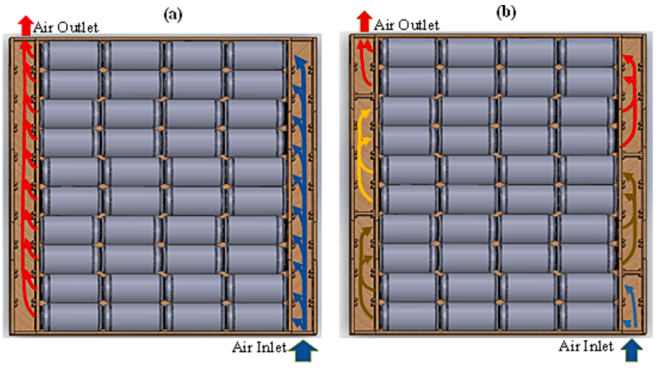

Fig. 1. Air pass configuration (a) Single-pass air heater (b) five-pass air heater.

2.2. Laboratory construction

The solar air heater is based on black-body radiation concepts that follow Stefan and Plank's laws. The aluminium cans are gathered, and the lids of the aluminium containers are perforated on both sides to allow air movement (Fig. 4). Medium-density fibreboard was used to construct the frame and the beverage containers were coated black and stacked in rows (see Fig. 5). The purpose of the black body is to absorb more thermal energy from the sun and raise the air temperature flowing through the aluminium cans through radiation, conduction, and convection. The single-pass air heater would have only one inlet manifold and one exit manifold (Fig. 1a). The multi-pass air heater, on the other hand, would have baffles at each end that would reverse the airflow direction depending on the required air pass (Fig. 1b and Fig. 2). In the final arrangement, the air heater is equipped with an angle adjuster in order to tilt the system at a different angle for maximum solar exposure (Fig. 6).

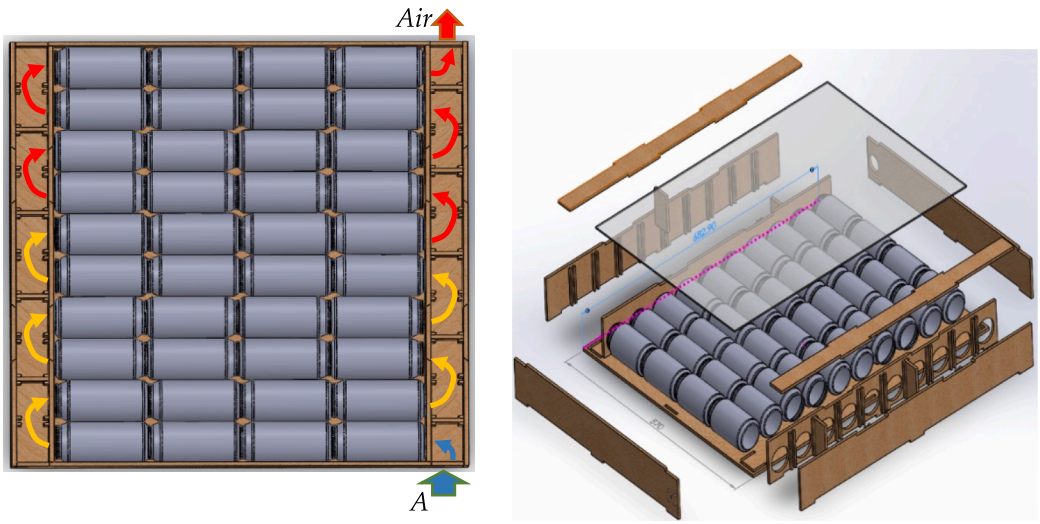

Fig. 2. (a) Ten-pass air heater configuration (b) Exploded view of system frame and aluminium cans arrangement.

2.3. Instrumentation and calibration

For this experiment, artificial solar lamps were utilised as the primary source of illumination. These lamps were capable of generating maximum irradiance of 750 W/m^2. The choice to use solar lamps was primarily due to their controllability, which proved advantageous for the execution of the experiment. Additionally, the period of experimentation was characterised by low solar irradiance, further necessitating the use of artificial lighting.

The data for the experiment was logged using a Squirrel SQ2040-2F16 data logger. This device was equipped with a K-type thermocouple, which has an error margin of ± 2.2 °C or 0.75 % (whichever is larger). This ensured that the data collected was both accurate and reliable.

Prior to the commencement of the experiment, all instruments were calibrated to ensure their precision and accuracy. The calibration process was thorough, minimising any potential errors or discrepancies in the data collected.

It is important to note that all experimental procedures were carried out with strict adherence to safety protocols and guidelines. This ensured not only the integrity of the data but also the safety of all personnel involved in the experiment.

3. Mathematical modelling

Fig. 7 shows a schematic configuration of the solar absorber collector and the aluminium cans arrangement below the glass cover, with labels.

The model formulation applies the conditions given by Duffie and Beckman [17]. The following assumptions considered to simplify the model are highlighted below;

- Steady-state operation
- No air leakage or the edge losses from the system
- The temperature drop across the glass cover is considered negligible
- The air temperature varies only across the fluid flow direction.

The schematic diagram is examined section by section (see Figs. 8, 9, 10 and 11).

3.1. Energy balance equations

Given below is the general energy flow between the surfaces.

$$q = \frac{Q}{A} \tag{1}$$

Where q is the rate of heat transfer per unit area.

3.1.1. Glass cover

$$I \bullet \gamma_g + \overline{q}_c + q_c = q_w + \overline{q}_d \tag{2}$$

$$I \bullet \gamma_g + \overline{h}_b(T_c - T_g) + \dot{h}_b(T_c - T_g) = (h_w + \overline{h}_d) \bullet (T_g - T_{am})$$

Where γ_g represent the absorptivity of the glass cover (Perspex), h_w is the heat transfer coefficient due to wind flowing over the glass cover, $\overline{h}_d$ is the heat transfer coefficient between the ambient and glass cover. $\overline{h}_b$ and $\dot{h}_b$ are radiative and convective heat transfer coefficients on the glass cover (Perspex).

3.1.2. Aluminium can (Topside)

$$I \bullet \tau_g \bullet \gamma_c = \overline{q}_c + q_c + \overline{q}_a + q_a \tag{3}$$

$$I \bullet \tau_g \bullet \gamma_c = \overline{h}_b(T_c - T_g) + \dot{h}_b(T_c - T_g) + \dot{h}_a(T_c - T_f) + \overline{h}_a(T_c - T_e),$$

Where τ_g and γ_c denote the transmissivity of the Perspex and absorptivity of the aluminium can, respectively. $\dot{h}_a$ and $\overline{h}_a$ are the convective and radiative heat transfer coefficient of the aluminium can.

3.1.3. Aluminium can (Bottom Side)

$$q_e + \overline{q}_a = q_i + q_a^{'} \tag{4}$$

$$\frac{\lambda_c}{x_c}(T_c - T_e) + \overline{h}_a(T_c - T_e) = \dot{h}_a^{'}(T_e - T_f) + U_e(T_e - T_i)$$

Where λ_c and x_c denote the thermal conductivity (W/(m·K)) and thickness (m) of the aluminium can. U_e is the heat loss coefficients of the Medium-density fibreboard (MDF) and $\dot{h}_a^{'}$ is the convective heat transfer coefficient coming from the bottom side of the aluminium can.

3.1.4. Air

For a single aluminium airflow

$$q_a + q_a^{'} = 2(\dot{m}c_p/A_{al})(T_f - T_1) \tag{5}$$

$$\dot{h}_a(T_c - T_f) + \dot{h}_a^{'}(T_e - T_f) = 2(\dot{m}c_p/A_{al})(T_f - T_1),$$

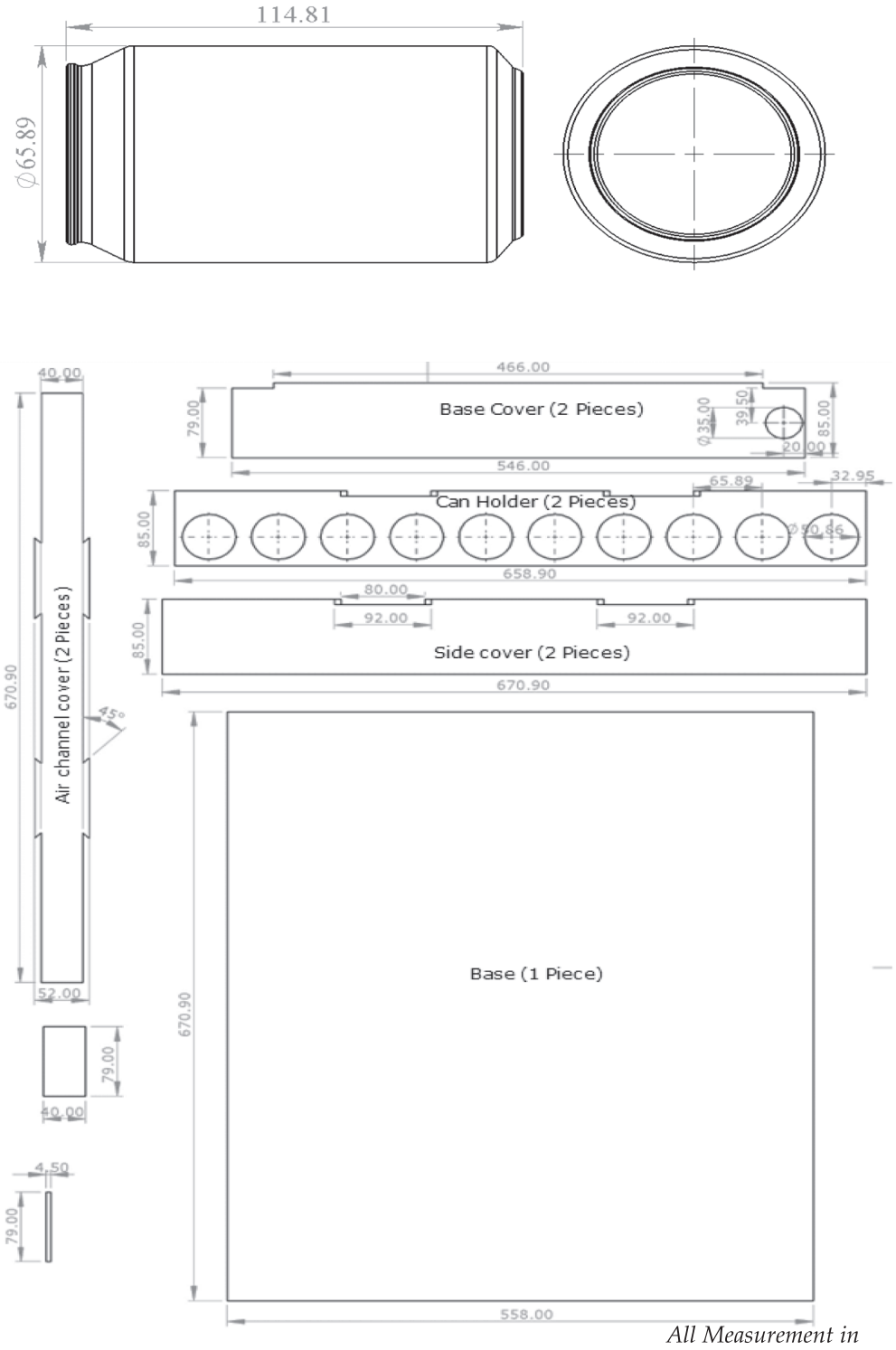

Fig. 3. (a) Aluminium Can Model (b) Dimension of MDF (wood) frame.

3.2. Determination of heat transfer coefficients

3.2.1. Radiation heat transfer coefficients

The heat transfer coefficients can be calculated using Watmuff et al. [43] and Duffie and Beckman [17] energy flow equations.

The energy flow from glass cover to ambient air

$$\overline{h}_d = \sigma\varepsilon_g(T_g + T_s)(T_g^2 + T_s^2)\frac{(T_g + T_s)}{(T_g + T_{am})} \tag{6}$$

The energy flow from aluminium Can to the glass cover

$$\overline{h}_b = \frac{\sigma(T_c^2 + T_g^2)(T_c + T_g)}{\frac{1}{\varepsilon_c} + \frac{A_c}{A_g}\left(\frac{1}{\varepsilon_g} - 1\right)} \tag{7}$$

The energy flow from aluminium Can top to bottom

Table 1
Material cost (Some materials were purchased from eBay).

Material	Cost ($)
Medium-density fibreboard (MDF) (600 × 600 mm)	25.86
Perspex (670.9 × 454.0 mm)	25
Wood screws	2
Black paint	2
Aluminium Cans	Nil
Air Blower	2
Battery	2
Battery case and wiring	5
Total	**63.86**

$$\overline{h}_a = \frac{\sigma(T_c^2 + T_e^2)(T_c + T_e)}{\frac{1}{\varepsilon_c} + \frac{A_c}{A_e}\left(\frac{1}{\varepsilon_e} - 1\right)} \tag{8}$$

Energy flow due to wind flowing over the glass cover

$$h_w = 2.8 + 3.0V_w \tag{9}$$

Where V_w (m/s) is the wind velocity of the ambient air.

3.2.2. Convection heat transfer coefficients

- Heat transfer between the glass cover and aluminium cans.

The conductive heat transfer coefficient can be calculated using

$$\dot{h}_b = Nu_b \bullet \frac{\lambda_{air}}{L_b} \tag{10}$$

Where λ_{air} is the thermal conductivity of air, Lb is the space between the glass absorber and the Nu_b is the Nusselt number for the air present in Lb. According to Duffie and Beckman [17], the Nusselt number can be calculated as given below;

$$Nu = 1 + 1.44\left[1 - \frac{1708(sin1.8\beta)^{1.6}}{Racos\beta}\right] \bullet \left[1 - \frac{1708}{Racos\beta}\right]^{+} + \left[\left(\frac{Racos\beta}{5830}\right)^{1/3} - 1\right]^{+} \tag{11}$$

Where β is the tilt angle, + exponent denotes that only positive values in the square brackets is applicable (i.e., square bracket value is zero when the term is negative), and Ra is the Rayleigh number which can be expressed with the equation below. [17],

$$Ra = \frac{g \bullet \beta' \bullet \Delta T \bullet L^3}{v_{air} \bullet \varphi_{air}} \tag{12}$$

Where g is the gravitational constant, β' is the volumetric coefficient of expansion, which is given as;

Fig. 4. Perforated Aluminium cans: (A) bottom side of can; (B) topside of can.

Fig. 5. Solar air heater assembly.

Fig. 6. Finished Solar air heater assembly.

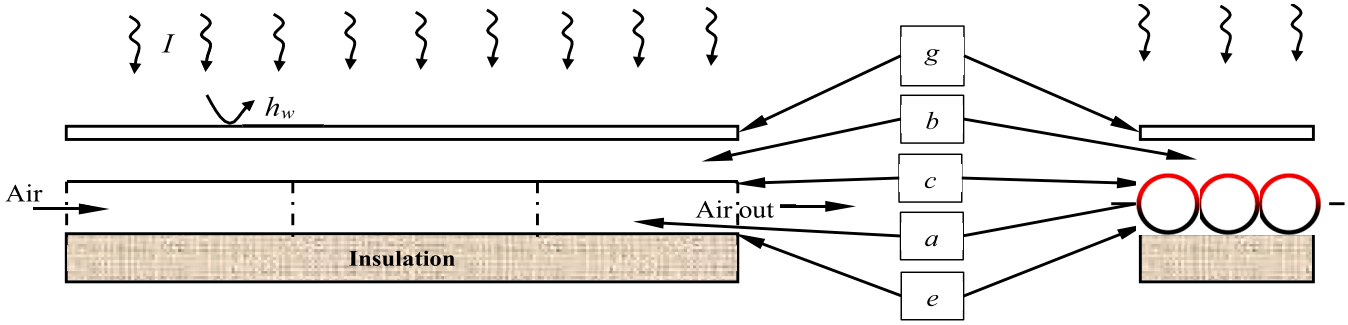

Fig. 7. Schematic diagram side and end view.

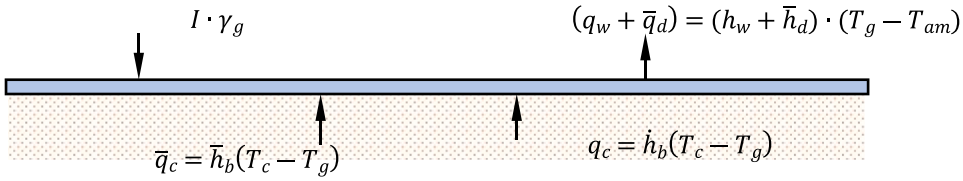

Fig. 8. Glass cover Energy flow.

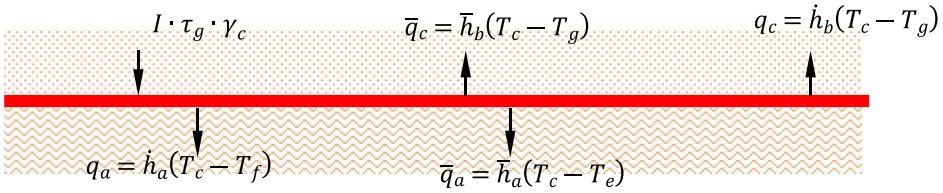

Fig. 9. Energy flow through the topside of the aluminium can.

$$= \frac{1}{T} \text{ and } T = (T_c + T_e)/2 \tag{13}$$

ν_{air} is the kinematic viscosity of air which is also given as μ/ρ and φ_{air} is the thermal diffusivity of air which is also given as $\lambda/\rho c_p$.

- For the convective heat transfer within the aluminium can.

$$\dot{h}_a = \dot{h}_a^{'} = Nu_a \bullet \frac{\lambda_{air}}{D_h} \tag{14}$$

Where Dh is the hydraulic diameter and is equal to the diameter of the aluminium can [17].

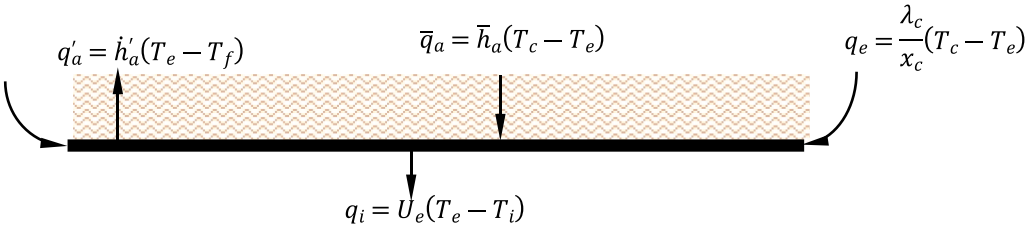

Fig. 10. Energy flow through the bottom aluminium can side.

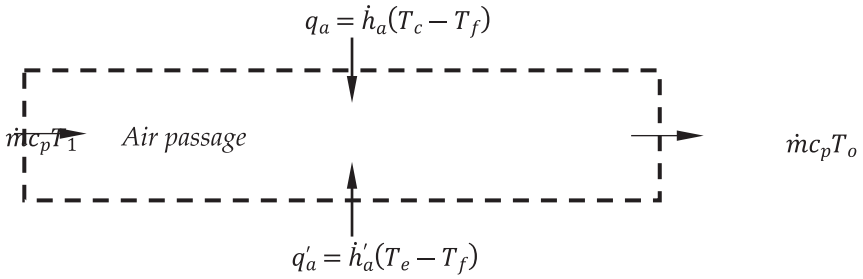

Fig. 11. Air flow through the aluminium cans.

Given below is the Laminal flow in a smooth duct and the local Nusselt numbers as presented by Heaton et al. [23]

$$Nu_a = Nu_\infty + \frac{i(Re \bullet Pr \bullet D_h/L)^m}{1 + j(Re \bullet Pr \bullet D_h/L)^n} \quad 15)$$

Where Re is the Reynolds, Pr is the Prandtl number and is given as 0.7 according to Cengel et al. [11].

Using the table given by Duffie and Beckman [17], the expression is calculated as given below

$$Nu_a = 4.4 + \frac{0.00398(0.7 \bullet Re \bullet D_h/L_1)^{1.66}}{1 + 0.00114(0.7 \bullet Re \bullet D_h/L_1)^{1.12}} \quad (16)$$

For turbulent flow in a smooth duct, the expression given by Dittus and Boelter [16] was used to determine the Nusselt number.

$$Nu_a = 0.00158Re^{0.8} \quad (17)$$

The equation below is used to calculate for Reynolds number (Re)

$$Re = \frac{\rho V_a D_h}{\mu} \quad (18)$$

Where Va is the mean air velocity, ρ is the density of air, Dh is the diameter of the aluminium can, μ is the dynamic viscosity.

For air temperature T (K) in the range of 280 – 470 K, Lin et al. [26] formulated an estimate for the density (ρ), thermal conductivity (λ) and dynamic viscosity (μ) of air below.

$$\rho = 3.9147 - 0.016082T + 2.9013 \times 10^{-5}T^2 - 1.9407 \times 10^{-8}T^3 \quad (19)$$

$$\lambda = (0.0015215 + 0.097459T - 3.3322 \times 10^{-5}T^2) \times 10^{-3}, \quad (20)$$

$$\mu = (1.6157 + 0.06523T - 3.0297 \times 10^{-5}T^2) \times 10^{-6}, \quad (21)$$

Lin et al. [26] noted that when using the expression above, c_p should be assumed to be 1000 J/kg K.

3.3. Thermal and Thermohydraulic efficiency

3.3.1.1 Thermal Efficiency

$$\eta_{th} = Q_c/IA_g \quad (22)$$

Where Q_c is the useful heat gain and can be calculated from the below expression.

$$Q_c = \dot{m}c_p(T_o - T_i) = 2\dot{m}c_p(T_o - T_i) \quad (23)$$

3.3.1.2 Thermohydraulic Efficiency.

Thermohydraulic efficiency, also known as the effective efficiency, is used to analyse the economic performance of the solar air heater by identifying how much energy is needed for the system to work.

$$\eta_{eff} = \frac{Q_c - (P_m/C)}{IA_g} \quad (24)$$

Where C is the conversion factor, which is the product of the efficiencies of the fan, electric motor, transmission, and thermoelectric conversion. The value of 0.07 will be used as recommended by Kumar and Chand [25]. P_m is the mechanical power needed to drive the air through the aluminium cans and it is given below

$$P_m = \dot{m} \bullet \Delta P/\rho \quad (25)$$

Where ΔP is the pressure drop across the airflow duct and is calculated by the given expression

$$\Delta P = \frac{4f\rho L_1 V^2}{2D_h} \quad (26)$$

Where f is the fanning friction factor, and according to Gupta and Kaushik [21], the expression

$$f = \frac{16}{Re} \text{ (for laminar flow)}, \quad (27)$$

$$f = 0.079Re^{-0.25} \text{ (for turbulence flow)}, \quad (28)$$

3.4. Mathematical Model Implementation in MATLAB

The equations were developed in the MATLAB workspace to evaluate the heat coefficients. Eqs. (2)–(5) can be solved simultaneously, but Eqs. (6)–(21) are dependent on each other and difficult to solve. Therefore, the Gauss-Seidel method, also known as the method of successive displacement, was adopted to solve these equations. Using random approximation, the iteration process selects values for the unknowns to obtain new sets of values. The process is repeated until the percentage

error of the present value and the last calculated value is less than ± 0.5 %. The solution process is shown in Fig. 12 and the design parameters for the analysis are listed in Table 2.

Step 1: Assume initial values for Tg, Tc, Te and Tf.

Step 2: Compute the properties of air in equations 3.19–3.21 using these values.

Step 3: Compute the various heat transfer coefficients using Eqs. (6)–(18).

Step 4: Input the calculated heat transfer coefficients into Eqs. (2)–(5) and solve simultaneously to obtain new values of Tg, Tc, Te, and Tf.

Step 5: Check the absolute difference between the newly obtained values and previous values to see if the solution has converged with an error of less than ± 0.5 %.

Step 6: If the solution has not converged, repeat the iteration from step 2 above using the newly obtained values. The iteration step is repeated until the solution converges with a ± 0.5 % error.

4. Results

This section presents both the simulation and experimental results, and discusses the performance of the solar air heater for different configurations. The three main aspects considered were output air temperature, mass flow rate, and thermal efficiency for the three design configurations. These parameters aided in determining the optimum design and configuration for the solar air heater.

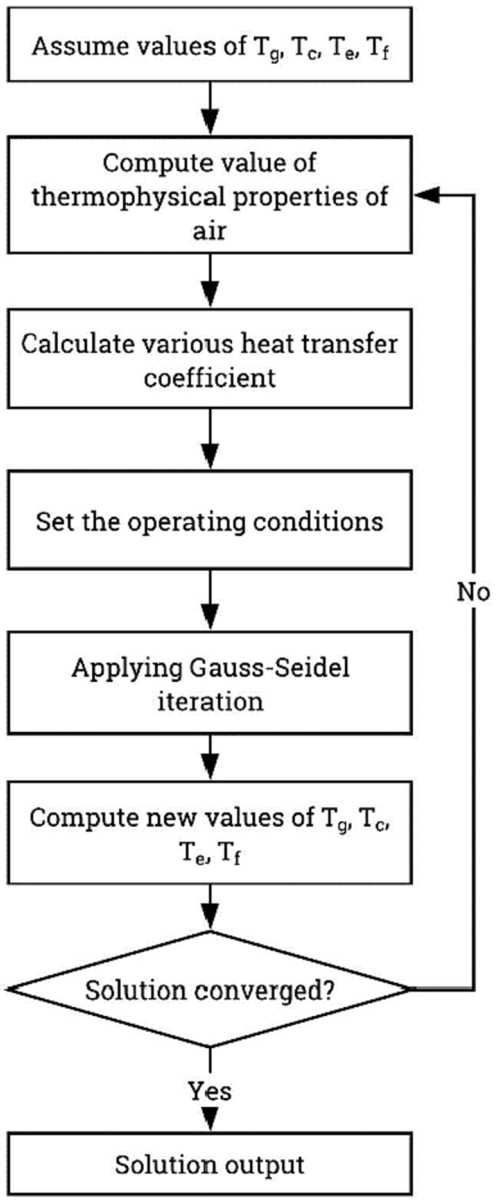

Fig. 12. Flow Chart of algorithm.

Table 2
Design and operating parameters of the solar air heater used for the analysis.

Parameters	Units	Value
Length of each aluminium can L_b	m	0.11504
The diameter of each aluminium can is D_h	m	0.06589
Spacing between the glass cover and aluminium can	m	0.040
Thermal conductivity of the Aluminium can λ_c_c [19]	W/mK	205
Heat loss coefficient of MDF U_e	W/m^{2}K	0.02
Absorptivity of the aluminium can		0.96
Absorptivity of the glass cover (Perspex)		0.10
Transmissivity of the glass cover (Perspex)		0.88
The emissivity of the aluminium can		0.95
The emissivity of the glass cover (Perspex)		0.90
The tilt angle of the collector	°	0
Ambient temperature	K	294
Inlet temperature	K	288
Solar Insolation	W/m^2	750
Specific heat capacity of air c_p	J/kgK	1000
Heat loss coefficient of MDF	W/m^{2}K	50
Stephan-Boltzmann constant	W/m^{2}K^4	5.67 × 10^{-8}

4.1. Simulation results

The increase in the number of aluminium cans increases the output air temperature, as shown in Fig. 14(a). However, the thermal efficiency decreases. The output temperature line versus quantity of aluminium graph is almost linear, while the thermal efficiency continues to decrease as the number of cans and flow path increases. Fig. 14(a) graphs alone do not seem to theoretically relate to each other, because the output temperature line graph should not be partially linear while the thermal efficiency graph remains nonlinear, as observed by Alvarez et al. [5,28] and [25]. However, the result can be explained by the graph of mass flow rate versus heat transfer coefficient in Fig. 14(b). The convection heat transfer coefficient through the 40 cans increases with the increase in the mass flow rate, which is attributed to the high flow velocity through the aluminium cans.

Additionally, considering the air temperature rise across each aluminium can (20, 30, 39, 45, 49 °C) and the air temperature of each can (10, 9, 6, 4 °C), as seen in Fig. 13, the air temperature drops non-linearly, while the solar aluminium cans absorption area increases linearly. Therefore, the heat loss is increased at elevated temperatures, and the rate of heat gain is decreased.

Fig. 15(a) shows that thermal efficiency increases with mass flow rate. However, outlet air temperature decreases with mass flow rate, as shown in Fig. 15(b). This is because the non-prohibitive airflow does not provide sufficient fluid mixing, which causes a drop in thermal efficiency. The ten-pass configuration system shows an improved air output temperature, which delivers better thermal heat.

4.2. Experimental results

Artificial solar lamps were used to generate solar light because the study was conducted during the winter season, when the solar intensity is lower than in other seasons. The lamps were also used to ensure a consistent and controllable solar intensity throughout the study. The lamps generated an average of 750 W/m^2, which is a similar solar intensity to that found in the summer season.

4.2.1. Thermal Infrared Imagery

The Fig. 16 is thermal imaging employed to detect regions of concentrated thermal heat within the system. There is a substantial heat

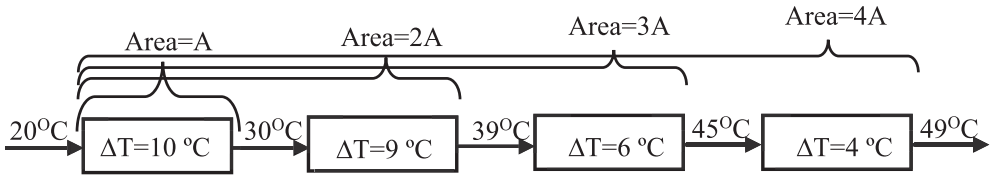

Fig. 13. Energy flow interaction as a function with area and temperature.

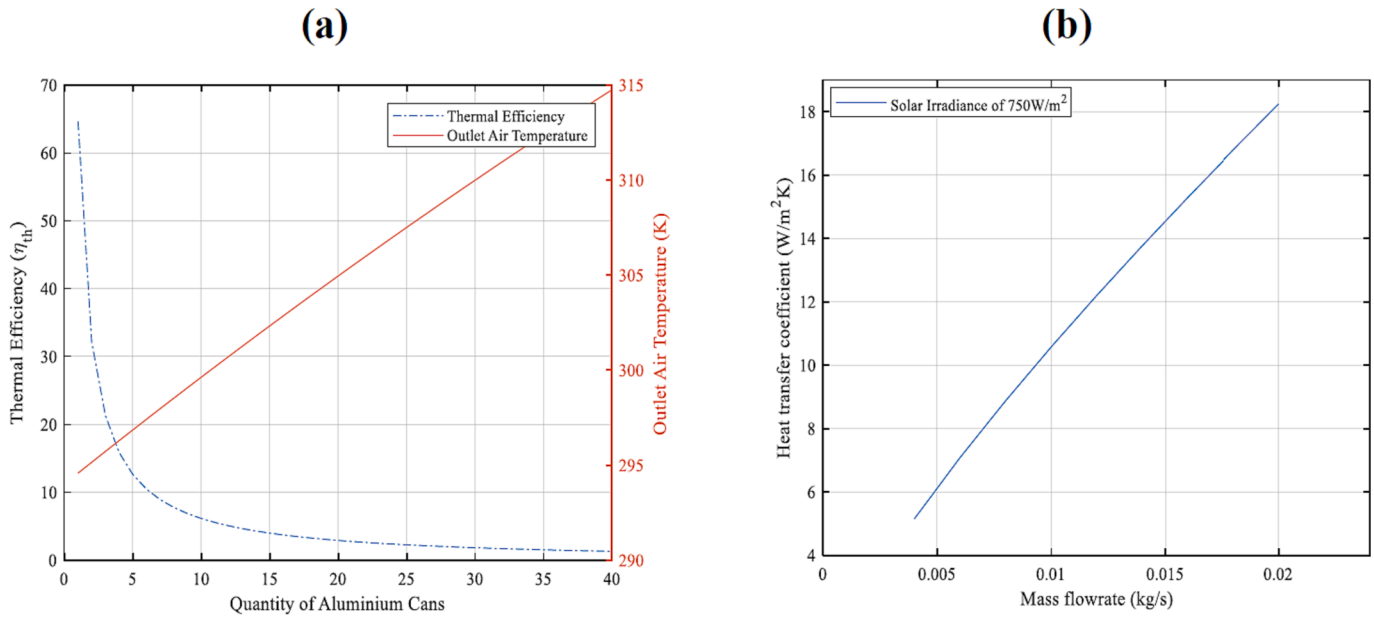

Fig. 14. (a) Thermal efficiency and temperature vs quantity of aluminium cans used; (b) Output temperature against mass flowrate.

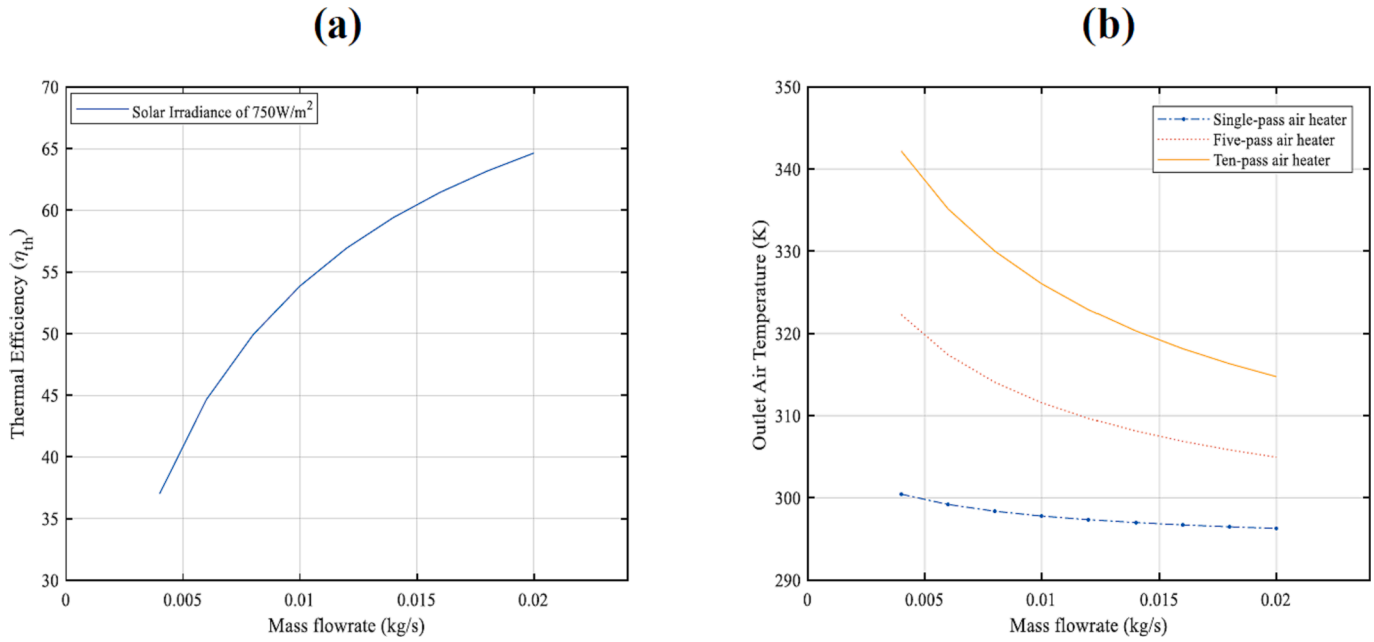

Fig. 15. (a) Thermal Efficiency against mass flowrate (b) Output temperature against mass flowrate.

loss around the system which will decrease the efficiency, resulting in a reduction of the usable heat delivered at the outlet. Future study can consider insulating the device because poor insulation can cause rapid heat loss to the surroundings during low solar intensity [6].

4.2.2. *Natural convection*

Using natural convection with solar irradiance of 750 W/m^2, different configurations were analysed. The ten-pass configuration (Fig. 19) delivers the highest heat gain among the three configurations,

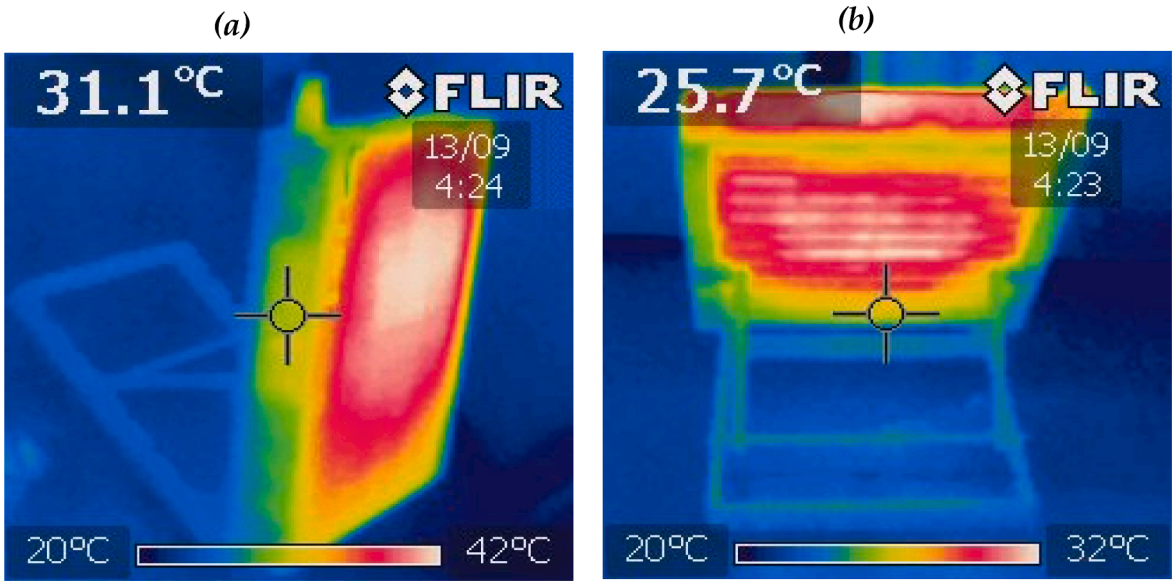

Fig. 16. Thermal Infrared Imagery while in operation; (a) Side view (b) Back view.

followed closely by the five-pass system (Fig. 18), which slightly outperforms the single-pass system (Fig. 17). At first glance, the ten-pass configuration may appear to be the most straightforward choice. However, a simulation analysis of the pressure loss in both multi-pass systems (Fig. 21) indicates that to increase airflow rate within the ten-pass configuration, it would necessitate a motor with a higher horsepower which does not correspond to a significant gain in useful heat. This factor is crucial to consider when evaluating the overall efficiency and feasibility of each configuration.

Table 3 shows the summary of the experimental results. While an increase in the number of passes leads to a rise in the outlet temperature, it's important to note that this increase in passes does not directly translate to a proportional increase in heat gain. This suggest that the number of air passes, mass flow rate and useful heat gain are all important factors that affect the performance of solar air heater systems.

4.2.3. *Forced convection*

A forced convective system was achieved using a PV-powered induction fan to increase the mass flow rate. The Fig. 20 illustrates that an increase in the mass flow rate leads to a decrease in air temperature. This is because the higher the mass flow rate, the lower the heat removing capacity. Following the pressure loss analysis for the multi-pass configurations in Fig. 21, it was observed that the pressure loss in the ten-pass configuration was significantly high (approximately double that

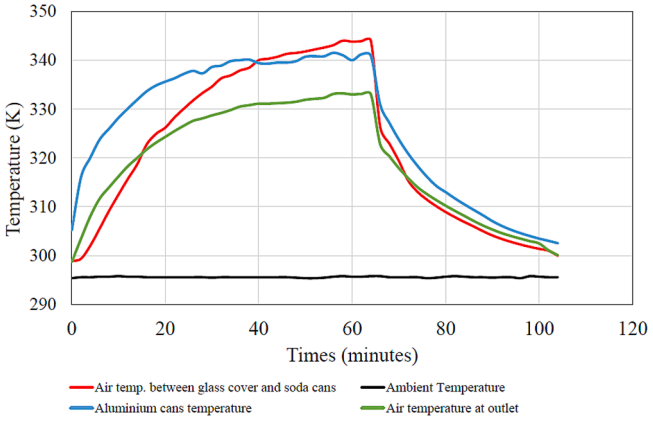

Fig. 17. Single-pass solar air heater.

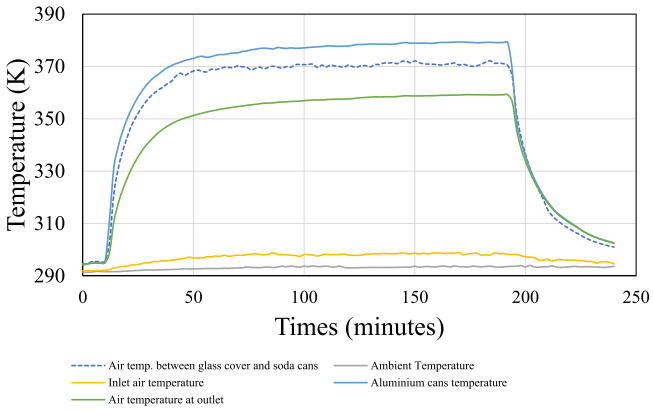

Fig. 18. Five-pass natural convective solar air heater.

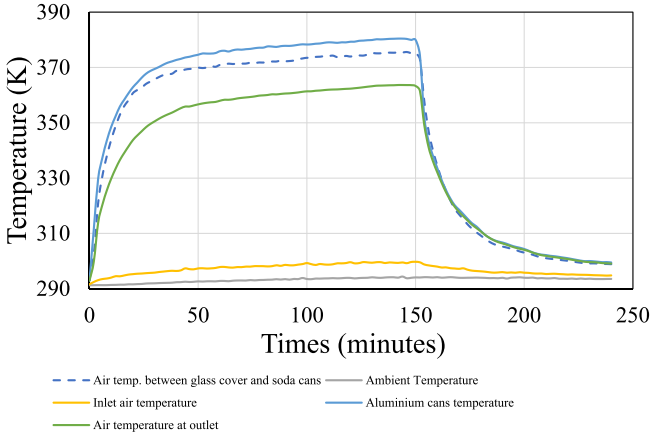

Fig. 19. Ten-pass natural convective solar air heater.

of the five-pass configuration) with minimal observed benefits in air temperature. In addition, this increased pressure loss increases the energy required to maintain airflow, necessitating a higher cost horsepower air blower which contradicts the research objective of developing a low-cost solution.

Table 3
Values of natural convective solar air heater.

Configuration	Maximum air temperature at the outlet (K)	Time to attain maximum temperature (minutes)	Mass flowrate (kg/s)	Heat gain (J/s)
Single-pass	333.20 (60.20 °C)	54	0.00038	14.83
Five-pass	359.23 (86.23 °C)	146	0.00045	29.28
Ten-pass	363.63 (90.63 °C)	150	0.00047	32.65

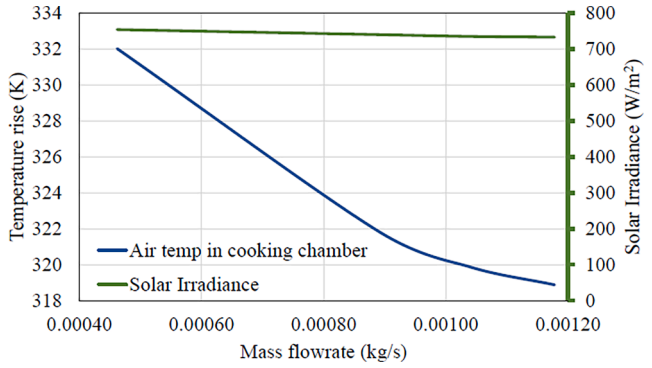

Fig. 20. Variation of air temperature rise against the mass flowrate for five-pass air heater.

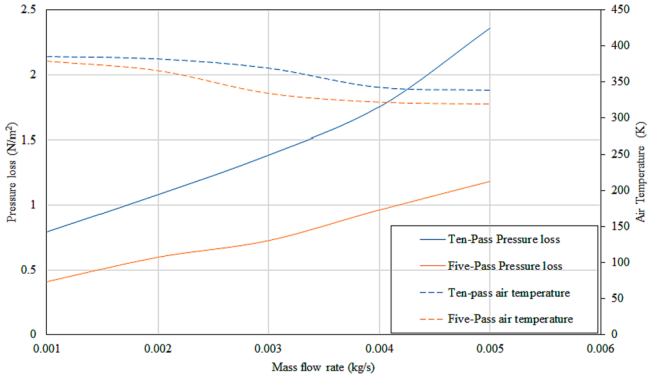

Fig. 21. Simulation of mass flow rate against pressure and air temperature.

4.4. Cost and implication

The modelled solar air heater was compared with other low-cost solar air heaters reported in recent literature (Table 4). The cost of production and the output temperature were compared. The developed model's production cost is in the range of the cheap models in the literature, owing primarily to the use of free beverage aluminium cans. Likewise, the outlet temperature of the system was also high than others (Table 4). The current model of the solar air heater has already been used for agricultural drying purposes like fish drying (data not included in this study). Other purposes can include home heating, slow cooking, etc. The system can be scaled up depending on the use. For instance, the output temperature can be increased if insulated materials are used to minimise heat loss from the MDF at observed in Fig. 16. The number of the aluminium cans can also be increased.

Apart from the low cost, which can be a benefit to low-income regions, another implication of creating this type of system is the benefit of utilising waste aluminium beverage cans. Waste beverage soda cans are a major environmental problem in low-income countries [40,13]. The environmental impact in these regions is currently a major topic of discussion [31,2,10], and ways to address it are currently being developed [7,15,2]. Overall, the use of waste aluminium beverage cans in this solar air heater system is a win–win for both the environment and low-income communities. It will provide a low-cost way for heating while reducing pollution and conserving resources.

Table 4
Low-cost solar heater in literature.

Low-cost solar air heater	Reference	Output temperature (K)	Cost ($)
Current air heater	NA	359.23 (86.23 °C)	63.86
Hybrid solar air heater	[27]	No data	67.25
Helical tubes, solar air heater	[37]	325.65 (52.5 °C)	67.00
Hybrid Model-1	[4]	345.35 (72.2 °C)	59.50
Hybrid Model-2	[4]	347.05 (73.9 °C)	57.50
Hybrid Model-3	[4]	344.95 (71.8 °C)	57.00

5. Validation and limitation of simulation results

The study was validated by comparing the mathematical model and experimental results. The results showed that the air temperature of both the model and the experimental results decreased with the increase in mass flow rate (Fig. 22(a)). However, the air temperature of the experimental results decreased at a higher rate than the mathematical model simulation results. In Fig. 22(b), the slope gradients of the two results are slightly equal, but the air temperature of the mathematical model simulation is higher than the experimental results.

The above observations can be attributed to the following factors:

- **Air leakage and edge losses:** The solar air heater was not tested in a completely sealed environment. This means that there was some air leakage, which would have reduced the efficiency of the system. In addition, the aluminium cans contain a reduction in the cross-sectional area which was not accounted for in the mathematical model simulation. The mathematical model simulation also assumed no air leakage and edge losses, so the results are higher than the actual results.
- **Artificial solar lamps:** The study used artificial solar lamps to simulate the solar radiation. These lamps are known to radiate less energy than direct solar sunlight. This would have reduced the temperature of the air in the solar air heater, resulting in lower experimental results [41].
- **Heat transfer coefficients:** The mathematical model simulation used heat transfer coefficients from the ambient wind flowing and the sky temperature. These values were not available during the laboratory experiment because the experiment was conducted indoors. This would have affected the accuracy of the mathematical model simulation results.
- **Heat loss at the baffle:** The mathematical model simulation did not include the heat loss occurring at the baffle on the solar air heater. This would have affected the performance of the experimental model, resulting in lower experimental results.

6. Conclusions

An analytical analysis was conducted using the Gauss-Seidel method, with MATLAB employed for the mathematical simulation, to model the thermal and fluid flow properties of a low-cost solar absorber system. The system utilised upcycled aluminium beverage cans, serving dual roles as both the solar absorber surface and the air duct. The study explored different configurations, including single-pass and multi-pass (that is, five and ten-pass) applications, and used parametric design techniques to determine the optimal configuration for the solar air heating application. The analytical study was validated through experimental testing. Additionally, a comparative cost analysis was

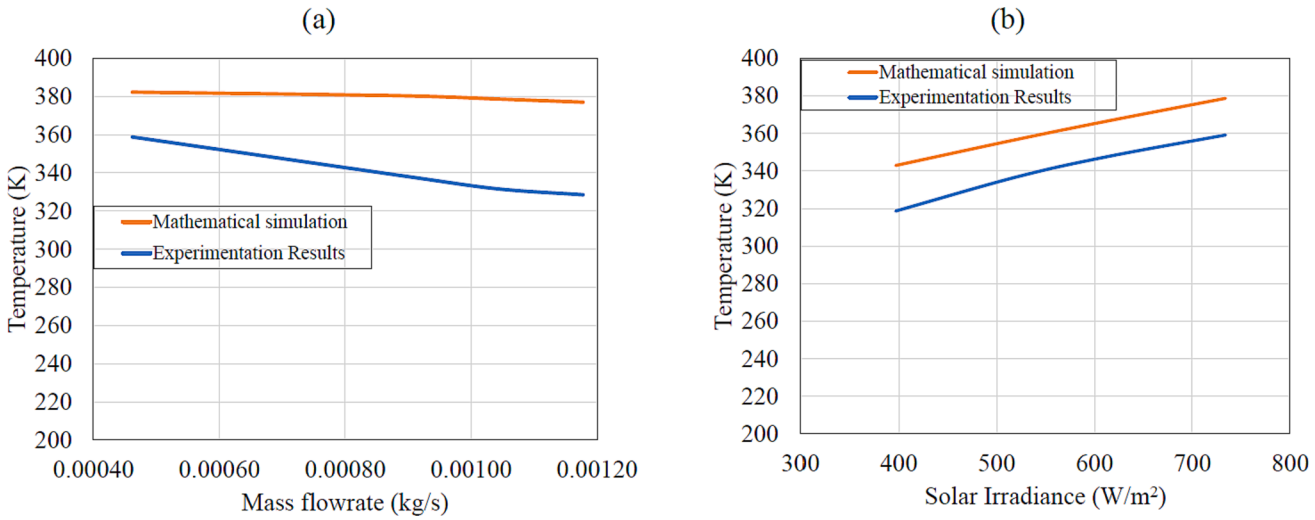

Fig. 22. (a) Air temperature against mass flow rate, (b) Air temperature against Irradiance.

performed by comparing the construction cost of this model with existing solar air heaters documented in recent literature.

The ten-pass configuration was found to deliver the highest heat gain among the configurations, followed closely by the five-pass system, which slightly outperforms the single-pass system. However, the pressure loss for a ten-pass configuration air heater is lower than that of the five-pass configuration, indicating that a higher pass configuration does not necessarily correspond to a significant gain in useful heat.

Other findings in the study are presented below:

- The air temperature rose and peaked at around 363.63 K (90.63 °C) in 146 min for the ten-pass air heater configuration and delivered 29.28 kg/s, while the five-pass peaked at 359.23 K (86.23 °C) in 150 min and delivered 32.65 kg/s. The airflow was natural convective using artificial solar lamps that generated an average of 750 W/m^2 irradiance.
- Heat up times for both multi-pass configurations were close; 146 min (2hrs, 26 min) for the ten-pass air heater and 150 min (2hrs, 30 min) for the five-pass air heater.
- A solar air heater made from waste aluminium beverage cans would provide an affordable heating solution for low-income regions. In terms of cost and performance, the model presented in this study is low cost compared to others in the literature while also capable of delivering high heat.
- Furthermore, the implementation of this system promotes the recycling of aluminium cans, contributing to effective solid waste management. This study not only provides a viable solution for harnessing solar energy but also addresses environmental concerns by upcycling waste aluminium cans.

In summary, this research underscores the potential of repurposing waste aluminium materials to create affordable and efficient solar heating solutions, with far-reaching implications for both energy management and waste reduction. The findings of this study are expected to provide valuable insights for future investigations in this field, particularly in the context of sustainable and renewable energy solutions.

CRediT authorship contribution statement

Emmanuel Omotosho: Investigation, Methodology, Software, Validation, Formal analysis, Writing – original draft, Writing – review & editing. **Philip Hackney:** Conceptualization, Project administration, Resources, Supervision, Investigation, Methodology, Software, Validation.

Declaration of competing interest

The authors declare that they have no known competing financial interests or personal relationships that could have appeared to influence the work reported in this paper.

Data availability

No data was used for the research described in the article.

References

[1] K.R. Abbasi, M. Shahbaz, J. Zhang, M. Irfan, R. Alvarado, Analyze the environmental sustainability factors of China: The role of fossil fuel energy and renewable energy, Renewable Energy 187 (2022) 390–402.
[2] Z. Al-Shatnawi, S. Alnusairat, A. Kakani, Towards zero solid waste in Jordanian universities: The case of Al-Ahliyya Amman University, Environ. Res. Eng. Manag. 76 (4) (2020) 46–59.
[3] T. Alam, M.-H. Kim, Performance improvement of double-pass solar air heater – A state of art of review, Renew. Sustain. Energy Rev. 79 (2017) 779–793.
[4] S. Algarni, V. Tirth, A. Saxena, P. Gupta, A comparative study of different low-cost sensible heat storage materials for solar air heating: an experimental approach, Energy Sources Part A 44 (1) (2022) 912–933.
[5] G. Alvarez, J. Arce, L. Lira, M.R. Heras, Thermal performance of an air solar collector with an absorber plate made of recyclable aluminum cans, Sol. Energy 77 (1) (2004) 107–113.
[6] M.M. Ardehali, M. Shahrestani, C.C. Adams, Energy simulation of solar assisted absorption system and examination of clearness index effects on auxiliary heating, Energ. Conver. Manage. 48 (3) (2007) 864–870.
[7] M.V. Barros, R. Salvador, C.M. Piekarski, A.C. de Francisco, Mapping of main research lines concerning life cycle studies on packaging systems in Brazil and in the world, Int. J. Life Cycle Assess. 24 (8) (2019) 1429–1443.
[8] T.M. Belay, S.M. Atnaw, W.-H. Chen, CFD Simulations and Experimental Investigation of a Flat-Plate Solar Air Heater at Different Positions of Inlet and Outlet, Journal of Renewable Energy 2023 (2023) 1–16.
[9] N.S. Bhatt, M. Yadav, Performance Analysis of Solar Air Heater with Finned Vertical Absorber, International Research Journal of Engineering and Technology (IRJET) 05 (04) (2018).
[10] A.C. Byers, T. Gustafsson, M. Shrestha, et al., A Sustainable Solid Waste Management Plan for Sagarmatha (Mt Everest) National Park and Buffer Zone, Nepal. Mountain Research and Development 40 (3) (2020) A1–A9.
[11] Y. Cengel, A. Ghajar, M. Kanoglu, Heat and mass transfer, McGraw Hill Higher Education, New York, 2011.
[12] F. Chabane, N. Moummi, S. Benramache, D. Bensahal, O. Belahssen, Collector Efficiency by Single Pass of Solar Air Heaters with and without Using Fins, Engineering Journal 17 (3) (2013) 43–55.
[13] B.C. Chukwudi, M.B. Ogunedo, Glass recycling: achieving a compromise between economics of production and environmental benefit, International Journal of Research and Review (IJRR) 6 (6) (2019) 391–396.
[14] P.M. Cuce, A. Saxena, E. Cuce, Y.N. Yilmaz, S. Shaik, S. Guo, Thermodynamic performance analysis of a low-cost, recycled and energy-efficient solar air heater with waste beverage cans: An experimental research, J. Therm. Sci. 32 (4) (2023) 1657–1670.

[15] M. Demartini, C. Pinna, B. Aliakbarian, F. Tonelli, S. Terzi, Soft drink supply chain sustainability: A case based approach to identify and explain best practices and key performance indicators, Sustainability 10 (10) (2018) 3540.
[16] Dittus FW and Boelter LMK (1930) University of California Publications on Engineering 2.
[17] J. Duffie, W. Beckman, Solar engineering of thermal processes, John Wiley & Sons, Hoboken, N.J., 2006.
[18] M. Gholikhani, H. Roshani, S. Dessouky, A.T. Papagiannakis, A critical review of roadway energy harvesting technologies, Appl. Energy 261 (2020), 114388.
[19] H.K. Ghritlahre, Performance evaluation of solar air heating systems using artificial neural network, National Institute of Technology, Jamshedpur, India, 2019.
[20] H.K. Ghritlahre, M. Verma, J.S. Parihar, D.S. Mondloe, S. Agrawal, A detailed review of various types of solar air heaters performance, Sol. Energy 237 (2022) 173–195.
[21] M.K. Gupta, S.C. Kaushik, Exergetic performance evaluation and parametric studies of solar air heater, Energ. Conver. Manage. 33 (11) (2008) 1691–1702.
[22] H. Hassan, S. Abo-Elfadl, M.F. El-Dosoky, An experimental investigation of the performance of new design of solar air heater (tubular), Renew. Energy 151 (2020) 1055–1066.
[23] H.S. Heaton, W.C. Reynolds, W.M. Kays, Heat Transfer in Annular Passages. Simultaneous Development of Velocity and Temperature Fields in Laminar Flow. International Journal, Heat Mass Transfer 7 (7) (1964) 763–781.
[24] C.M.S. Kumar, S. Singh, M.K. Gupta, Y.M. Nimdeo, R. Raushan, A.V. Deorankar, T. M.A. Kumar, P.K. Rout, C.S. Chanotiya, V.D. Pakhale, A.D. Nannaware, Solar energy: A promising renewable source for meeting energy demand in Indian agriculture applications, Sustainable Energy Technol. Assess. 55 (2023), 102905.
[25] R. Kumar, P. Chand, Performance prediction of extended surface absorber solar air collector with twisted tape inserts, Solar e-Energy 169 (2018) 40–48.
[26] W. Lin, W. Gao, T. Liu, A parametric study on the thermal performance of cross-corrugated solar air collectors, Appl. Therm. Eng. 26 (10) (2006) 1043–1053.
[27] M.H. Masud, R. Ahamed, M. Mourshed, M.Y. Hossan, M.A. Hossain, Development and performance test of a low-cost hybrid solar air heater, Int. J. Ambient Energy 40 (1) (2019) 40–48.
[28] C. Mgbemene, I. Jacobs, C. Agbo, et al., Experimental Investigation on the performance of a solar air heater with the absorber plate made of aluminium soda cans. 35th National Solar Energy Forum, Solar Energy Society of Nigeria, Abuja, 2017.
[29] R. Moradi, A. Kianifar, S. Wongwises, Optimization of a solar air heater with phase change materials: Experimental and numerical study, Exp. Therm Fluid Sci. 89 (2017) 41–49.
[30] G. Murali, K. Rama Krishna Reddy, M.T. Sai Kumar, et al., Performance of solar aluminium can air heater using sensible heat storage, Mater. Today:. Proc. 21 (2020) 169–174.
[31] O. Owojori, J.N. Edokpayi, R. Mulaudzi, J.O. Odiyo, Characterisation, recovery and recycling potential of solid waste in a university of a developing economy, Sustainability 12 (12) (2020) 5111.
[32] M. Paterson, The end of the fossil fuel age'? Discourse politics and climate change political economy, New Political Economy 26 (6) (2021) 923–936.
[33] M.S.W. Potgieter, C.R. Bester, M. Bhamjee, Experimental and CFD investigation of a hybrid solar air heater, Sol. Energy 195 (2020) 413–428.
[34] N.A.A. Qasem, M.N. Arnous, S.M. Zubair, A comprehensive thermal-hydraulic assessment of solar flat-plate air heaters, Energ. Conver. Manage. 215 (2020), 112922.
[35] K. Rajarajeswari, P. Alok, A. Sreekumar, Simulation and experimental investigation of fluid flow in porous and non-porous solar air heaters, Sol. Energy 171 (2018) 258–270.
[36] G. Raju, M.M.J. Kumar, Experimental study on solar air heater with encapsulated phase change material on its absorber plate, Energy Storage 3 (5) (2021) e256.
[37] A. Saxena, N. Agarwal, E. Cuce, Thermal performance evaluation of a solar air heater integrated with helical tubes carrying phase change material, J. Storage Mater. 30 (2020), 101406.
[38] A. Saxena, Varun, A.A. El-Sebaii, A thermodynamic review of solar air heaters, Renew. Sustain. Energy Rev. 43 (2015) 863–890.
[39] S. Singh, Experimental and numerical investigations of a single and double pass porous serpentine wavy wiremesh packed bed solar air heater, Renew. Energy 145 (2020) 1361–1387.
[40] W.S. Soh, R. Ali, N.M. Abdullah, Eco-trap: An Innovative Low-Cost Trash Trap to Remove Solid Waste on River Surface, Progress in Engineering Application and Technology 2 (2) (2021), 1124–1129-1124–1129.
[41] L. Thorington, L. Parascandola, L. Cunningham, Visual and biologic aspects of an artificial sunlight illuminant, J. Illum. Eng. Soc. 1 (1) (1971) 33–41.
[42] D. Utazi, S. Audu, S u,, Optimization of a Solar Air Heater: A Review, Nigerian Journal of Solar Energy 32 (2021) 98–107.
[43] J.H. Watmuff, W.W.S. Charters, D. Proctor, Solar and wind induced external coefficients for solar collectors, COMPLES 2 (1977) 56.